Materials and Design 141 (2018) 276–285

Contents lists available at ScienceDirect

Materials and Design

journal homepage: www.elsevier.com/locate/matdes

High performance strain sensors based on chitosan/carbon black composite sponges

Yongwang Liu [1], Huanjun Zheng [1], Mingxian Liu *

Department of Materials Science and Engineering, Jinan University, Guangzhou 510632, PR China

HIGHLIGHTS

- Conductive chitosan (CS)/carbon black (CB) composite sponges were prepared by solution-mixing and freeze-drying.
- CB can form a continuous filler network in CS matrix.
- CB increased the electrical conductivity, compressive properties, and thermal stability of CS sponges.
- CS/CB composite sponges can detect various human activities such as pronouncing and breathing.

GRAPHICAL ABSTRACT

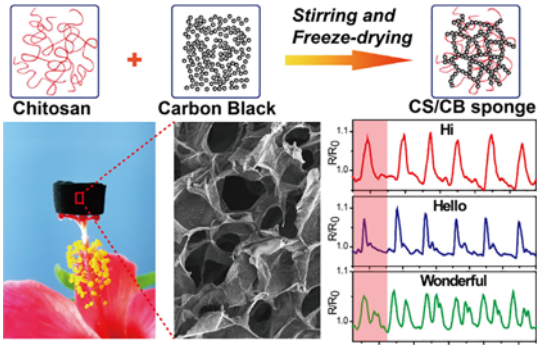

ARTICLE INFO

Article history:
Received 23 October 2017
Received in revised form 22 December 2017
Accepted 23 December 2017
Available online 26 December 2017

Keywords:
Chitosan
Carbon black
Sensor
Mechanical property
Structure
Sensitivity

ABSTRACT

Chitosan (CS)/carbon black (CB) composite sponges with high electrical conductivity and strain sensing sensitivity are prepared by combining solution-mixing and freeze-drying techniques. CB nanoparticles with diameter of ~40 nm play the role of a conductive component in the CS/CB composites. CB can form a continuous filler network in CS, which leads to the increase in viscosity and shear modulus. When writing and drying the CS/CB conductive ink, conductive tracks are obtained. With the increase in CB content, the density, electrical conductivity, compressive properties, and thermal stability of CS sponges are improved. The X-ray diffraction and Fourier transforms infrared spectroscopy results show CB are successfully compounded into CS matrix. The addition of CB leads to a slight decrease in the porosity of CS sponges. Sensing performances of CS/CB composite sponges are investigated by detecting various human activities including pronouncing, breathing, and joint bending. CS/CB composite sponges show good sensitivity and stability after several hundred loops. CS/CB composite sponges combine the advantages of low-cost, easy fabricating process, flexible, and high performance, which make them show great potentials in highly sensitive strain sensor.

1. Introduction

In the information age, the premise of making full use of information is to obtain accurate and reliable information, and sensors are main ways to access information in the field of natural and industrial production [1,2]. Flexible and sensitive strain sensors have considerable scientific, technological, and commercial significances in various applications such as sport motion monitoring [3], speech recognition [4], robot prosthesis [5], electronic skin [6], and portable healthcare monitors [7], etc. In recent years, various strain-sensing mechanisms including transistor sensing, capacitive sensing, piezoelectric sensing, triboelectric sensing, and resistive sensing, have been developed to construct sensitive strain

* Corresponding author.
E-mail address: liumx@jnu.edu.cn (M. Liu).
[1] These authors contributed equally to this work.

https://doi.org/10.1016/j.matdes.2017.12.046
0264-1275/

sensors [8–11]. Strain sensor is a force sensitive sensor based on the resistance-strain effect produced by stress deformation (compression, bending, or stretching) of an object. The so-called resistance-strain effect refers to the resistance of material will change when the deformation occurs. According to the resistance-strain effect, various conductive materials are used to design sensors by measuring the resistance changes when the objects occur deformation [12]. Up to now, strain sensors have been fabricated by employing carbon black (CB) [2], carbon nanotubes (CNT) [13], graphene [14], nanowires [15], and other conductive nanoparticles [16]. These conductive nanoparticles are further mixed with elastic polymer to prepare flexible and robust sensors. Although conductive composite for strain sensors have been extensively studied, some problems have yet to be solved for practical applications. For example, strain is hardly to be transferred into clear electrical signals due to the poor sensitivity of material. Moreover, instability and poor repeatability of these sensors usually result in measurement error. Besides, large-scale application of most existing strain sensor is limited to sophisticated preparing process and costly raw material such as metal nanoparticle and graphene.

CB is one of the most useful carbon materials used in several products, such as tires, plastics, electrostatic discharge compounds, pigmented coatings, toners and printing inks. CB is a semiconductor material with a volume resistivity of about 0.1 to 10 Ω · cm. The conductivity of CB is related to the large specific surface area and the graphitic character of their surfaces [17]. The raw materials of CB are easy to obtain, and the conductive properties of it are lasting and stability. Moreover, it can greatly adjust the resistivity of composite materials [18]. Therefore, the conductive composite made by CB is widely used as sensors [19–21]. The conductive mechanism of CB filler is complex, which mainly includes conductive channel, tunnel effect, and field emission theory [22]. Generally, CB is uniformly dispersed in matrices in the form of particles. As the amount of CB increases, the spacing among the particles decreases. When it comes close to or in contact state, a large number of conductive network channels are formed and the electrical conductivity is greatly improved. In addition, the higher the structure of CB, the easier the formation of space network access. The conductive network is not easy to be destroyed under normal conditions. For example, Wang et al. [23] successfully prepared CB-filled silicone rubber composite and find the piezoresistivity of composites with different CB content. Zhang et al. [24] prepared 3D hierarchical conductive structure of CB/natural rubber composites by incorporation of cellulose nanowhiskers via latex assembly technology and investigated the role of the hierarchical conductive structure on the liquid sensing behavior. Bhagavatheswaran et al. [25] constructed a strong filler–filler network in styrene butadiene rubber matrix by using the synergetic effect of micro-silica fume and CB, which can be used as a pressure sensor. Conventionally, elastomeric conductive composites are proved to be optimized sensing materials for piezoresistive sensors. However, some elastomeric composite materials are insensitive, unstable, and incapable of detecting low pressure. Therefore, porous CB based composite sponge with low density and rapid recovery rate are desirable for construction of strain sensors considering their electronic conductivity and mechanical flexibility.

In this work, we demonstrate a simple and cost-efficient strategy for fabricating flexible, highly sensitive, and versatile pressure-sensing platform based on CB and chitosan (CS) via solution-mixing and freeze-drying methods. CS is selected as the polymer matrix due to its easy processing into flexible sponge, high compressive property, environmentally friendly, and low cost. CB adhered to the molecular chain of CS and formed a continuous conductive pathway in the composite. The structure and properties of the composite solution and the porous sponges were examined. The conductivity and mechanical properties of the CS sponge are increased by the addition of CB, which is attributed to the uniformly dispersed conductive CB. The high sensitivity (gauge factor ≈7.5) and versatility of the CS/CB sponges in pressure sensing are attributed to the formation of conductive network channels. The versatile capabilities of this pressure-sensing platform in speech recognition, health monitoring (breathing), human activities detection (pronouncing, joint bending), and cycle stability test were also confirmed. The prepared CS/CB pressure sensors combine the advantages of simplicity, robust, low-cost, ultralow density, environmentally friendly as well as versatility in monitoring a wide range of pressure stimuli.

2. Experimental

2.1. Materials

Conductive carbon black (CB, BLACK PEARLS® 2000) was purchased from Cabot Corporation. It exhibited fine particle size and super high surface area with extremely high structure, which was commonly used for conductive or anti-static applications with high reinforcement properties. Chitosan (CS, Jinan Heidebai Marine Bioengineering Co., Ltd., China) had a degree of deacetylation of 85% and a viscosity (10 g/L, 20 °C) of 200 mPa.s. Glacial acetic acid and anhydrous ethanol were analytically pure and bought from Tianjin Fu Fine Chemical Co., Ltd., China.

2.2. Preparation of CS/CB composite sponges

The deionized water, CS powder, and glacial acetic acid were mixed at a mass ratio of 50:1:1 under stirring at room temperature for 12 h to obtain a clear CS solution. The CB powder was then added to the CS solution in the mass ratio of 25, 50, 100 and 200% (relative to the weight of CS). In order to make the dispersion be mixed uniformly, the CB at high loading (100 and 200%) was added with several times. The CS/CB solution was obtained after stirring at room temperature for 48 h, then the solutions were poured into 24-well plate and frozen for 8 h at −40 °C. After freeze drying for 24 h, the samples were removed from the 24-well plate using a syringe needle to obtain CB/CS composite sponges.

2.3. Preparation of CS/CB composite sponges for sensor device

The preparation process of CS/CB composite sponges for sensor device was basically consistent with the preparation procedure of CS/CB composite sponges. The only difference was that the mold used in freeze-drying was petri dishes. The lyophilized sample in thickness of 2–4 mm was cut into the appropriate shape according to the actual requirements of the characterization experiment.

2.4. Characterizations

2.4.1. Transmission electron microscopy (TEM)

0.01 wt% of CB ethanol dispersions were dropped in carbon membrane supported copper mesh and dried naturally. The morphology of CB particles was observed by Philips TECNAI 10 TEM, with magnifications of 39,000 X and 65,000 X.

2.4.2. ξ-potential and particle size analysis

The ξ-potential and particle size distribution of CB dispersions were measured via dynamic light scattering (DLS) using a Nano-ZS instrument (Malvern Instruments Ltd., UK). CB was dispersed in the anhydrous ethanol under ultrasonic treatment.

2.4.3. X-ray diffraction (XRD)

XRD patterns of CB, CS, and CS/CB composite sponges were determined by X-ray diffraction (Rigaku, Miniflex600, CuKα, Japan) at an accelerating voltage of 40 kV and the current of 40 mA.

2.4.4. Fourier transforms infrared spectroscopy (FTIR)

FTIR spectra were measured by infrared spectroscopy using attenuated total reflection (ATR) model in a NICOLET iS10 FT-IR Spectrometer. Thirty-two consecutive experiments were carried out and averaged.

The spectral scope ranged from 4000 to 500 cm^{-1} with a wavenumber resolution of 4 cm^{-1}.

2.4.5. Rheology

A rotational rheometer (Kinexus pro+, Malvern Instruments, Malvern, UK.) was used to measure the dynamic viscosity of the CS and CS/CB solution at room temperature at the shear rate of 1–100 s^{-1}. A dynamic frequency sweep test from 0.1 to 100 rad/s was taken to determine the dynamic shear modulus (G′, elastic component) of each solution.

2.4.6. Electrical conductivity determination

The conductivity of the cylindrical shape sample was measured with a multimeter (Fluke 17B+) (Fig. S1). The conductivity was calculated according to the following formula:

$$G = \frac{L}{RS} \quad (2-1)$$

where G is the conductivity, L is the length of the sample in the energized direction, R is the resistance of the sample, S is the cross-sectional area of the sample perpendicular to the direction of energization.

2.4.7. Porosity

The porosity of the sponges was measured by alcohol immersion method. The size and mass of the composite sponges were measured with a vernier caliper and an electronic balance to calculate the sample density. Then, the sample was immersed in anhydrous ethanol for 24 h. The mass of the sample was weighted after soaking with ethanol. The porosity was calculated according to the following formula:

$$\text{porosity} = \frac{W_2 - W_1}{\rho V_1} \times 100\% \quad (2-2)$$

where W_1 and W_2 are the weight of the sample before and after soaking, respectively; V_1 is the volume before immersion in alcohol and ρ is the density of alcohol.

2.4.8. Mechanical properties determination

The compressive mechanical behavior of composite sponges was measured by universal testing machine (UTM-Q422, Chende Jinjian Testing Instrument co., LTD, China). The test was performed at a strain rate of 2 mm/min. The maximum deformation was set as 80%.

2.4.9. Thermo gravimetric analyzer (TGA)

TGA of CS and CB/CS composite sponges was tested using the NETZSCHTG 209 F3 Tarsus under a nitrogen atmosphere from room temperature to 600 °C at a heating rate of 10 °C/min.

2.4.10. Scanning electron microscopy (SEM)

The pore structure of the sponges was characterized by scanning electron microscopy (Zeiss Ultra 55 SEM, Germany) at a voltage of 10 kV. Before observation, a thin gold layer was sprayed on the sample surfaces.

2.4.11. Performance of the strain sensor

The CS/CB composite sponge sample (50%) was cut into the appropriate shape according to the actual requirements for the characterization experiment. The current signals of the samples were recorded on insulation resistance tester (TEGAM 1740). To monitor the motion of fingers and joints, the sensor with 3 mm in width and 6 cm in length was mounted on fingers or joints by strong glue. During testing, the two terminals of the sensor were fixed on fingers or joints by 3M Scotch tape to avoid the resistance instability of the contact between the electrode and the sensor.

3. Results and discussion

3.1. Characterization of CB

The used conductive CB (BLACK PEARLS 2000) was an industrial product from Cabot Corporation. It is a furnace process CB which offers excellent conductivity and anti-static discharge properties at very low loadings in rubber compounds. Fig. 1A shows the TEM images of the CB. CB particles have a complicated structure with some spherical particles being fused together. The morphology of the CB is like grape-like aggregates with a single CB spherical particle diameter of about 40 nm. It is obvious that the CB exhibits a very fine particle sized, super high surface area, and extremely high structure. This unique interconnected structure of CB is beneficial to the formation of conductive network in polymer matrix. The particle size distribution of CB is shown in Fig. 1B. It can be seen that the CB displays a relatively narrow size distribution from 198.0 to 356.2 nm. The average size of CB in ethanol is 265.8 nm, and the zeta-potential of CB is +5.74 mV. Fig. 1C shows the XRD patterns of the CB particles. It can be seen that CB exhibits two diffraction peaks around 25.5° and 43° which is attributed to the (002) and (100) plane respectively [26]. The degree of crystallization of the carbon material is often described by the graphitization degree G, which is calculated as follows:

$$G = \frac{0.344 - d_{002}}{0.344 - 0.3354} \quad (2-3)$$

where d_{002} is the layer spacing calculated from the principal characteristic peaks (002) of the carbon material in the XRD pattern. The layer spacing of the CB is calculated as 0.3390 nm from Fig. 1C. The G value of the CB is determined as 58.11%, suggesting their high graphitization degree and high electric conductivity [27]. Fig. 1D shows the FTIR spectra of CB. The peaks appear at the wavenumber of 3450 (stretching vibration of OH group due to the adsorbed water and phenolic hydroxyl groups on the CB surfaces), 1635 (stretching vibration of C═O group), 1384 (bending vibration of C—H), and 1089 cm^{-1} (stretching vibration of C—O) are the characteristic peaks of the CB [28]. Fig. 1E shows the Raman spectra of the used conductive CB. CB exhibits two characteristic absorption peaks with intensity maxima at ~1350 and ~1580 cm^{-1} which are assigned to for sp^2 carbon disorder-induced D band and graphite G band respectively [29]. Also, a pronounced shoulder at ~2670 and a relatively weak peak at 2920 cm^{-1} can be seen in the spectra, which can be attributed to the $(2*D1)_2$ band and a combination of D and G modes characteristic for disturbed graphitic structures [30]. The surface area analysis was further carried out on CB by BET method. The surface area S_{BET} is determined as 75.75 $m^2\ g^{-1}$ in the region of relative pressure of 0.04–0.32. BJH pore size distribution curve of CB is shown in Fig. 1F. It can be seen the CB shows a peak around 2.6 nm in the pore width distribution curve, which suggests a mesopore structure on the CB surfaces [31]. The nano-sized CB facilitates the formation of a conductive network in the polymer matrix at low loadings.

3.2. Characterization of CS/CB dispersion

CB and CS were homogeneously mixed by solution mixing, and the resulting mixture solution was freeze-dried to prepare CS/CB composite sponges (Fig. 2A). CB can adhere to the molecular chain of polysaccharide and form a continuous conductive pathway in the composite sponges. Fig. 2B shows the appearance of pure CS and CS/CB solution. Pure CS solution is transparent and uniform liquid, while the CS/CB mixture displays homogenous black color with evenly dispersed CB after a long period of stirring. In general, CB is insoluble and hardly dispersed in water and organic solvents without any dispersant. However, CS is protonated in the acetic acid solution and the prepared CS solution is a high viscosity liquid. CS molecular chains have active groups of NH_2 and OH groups, and CS exhibit high adsorption capacity towards many

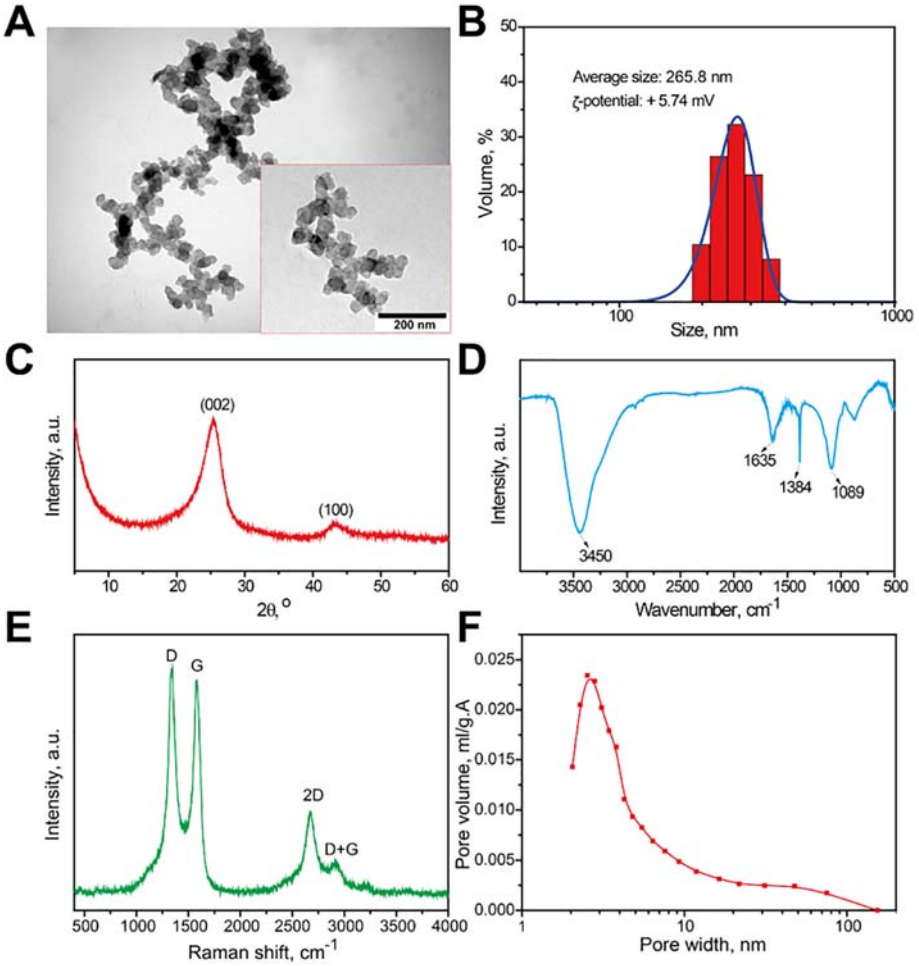

Fig. 1. TEM images of CB (inset is the enlarged TEM images) (A); Zeta potential and size distribution of CB in ethanol dispersion (B); XRD pattern of CB (C); FTIR spectra of CB (D); Raman spectra of CB (E); BJH pore size distribution of CB (F).

substances. Therefore, during the stirring process, the CB with high specific surface area and mesoporous structure can gradually adsorb on CS molecular chain. The prepared CS/CB dispersion has good stability and can be stored for several weeks without sedimentation. The rheological properties of the two solutions were subsequently studied. Fig. 2C shows the dependence of solution viscosity on shear rate. CS and CS/CB solution are non-Newtonian pseudoplastic fluids, and their viscosity decreases with the increase of shear rate. The shear thinning is related to the local orientation of CS chains due to the thixotropic effect. In addition, the molecular chains breakage during shearing can also cause the "pseudoplastic" phenomenon. The viscosity of the CS/CB solution decreases firstly and then increases with the increase of CB content. When the amount of CB is small, CB can disturb the entanglement of CS chains which is related to the hydrogen bond interactions among them. But when the loading of CB reaches more than 100%, the viscosity brought by CB itself cannot be ignored. As a result, the viscosity of the CS/CB solution is significantly improved. The shear modulus *G'* of the solution also reduces firstly and then increases with the increase of the amount of CB (Fig. 2D), which is consistent with the results shown in Fig. 2C. This may be because when the amount of CB is small, the CB nanoparticles makes the molecular chain easy to slip. Therefore, the entanglement decreases which result to the decreased in viscosity and shear modulus. When the CB particles reach a certain concentration, the CB aggregate builds a more compact network which is expected to result in the increase in the viscosity. In order to study the conductivity of the CS/CB solution, a rollerball pen with ball diameter of 1.0 mm was used to draw a clear track using the CS/CB ink on A4 common office paper (Fig. 2E). It can be seen that the tracks with width ~500 μm are conductive. A simple circuit was also written on A4 paper and linked with a LED (Fig. 2F). When it accesses to power, it can be seen that LED light bulbs give out light steady. These results suggest that CS/CB solution has good conductivity, which shows great promising applications in inkjet printing, circuit plate printing, and flexible screen printing. The paper with conductive tracks can also be used as flexible strain sensor due to the mechanical flexibility and light weight of paper [32].

3.3. The physical properties of CS/CB composite sponges

The effects of CB on the physical properties including the density, porosity, conductivity, and mechanical properties of CS sponge were investigated. Fig. 3A shows the appearance of the CS/CB sponges. It can be observed that the shape of the sponge is regular and the sponges are homogenous. The density of pure CS sponge and CS/CB composite sponge is very low. For example, the CS/CB sponges can easily stand on pistils of Hibiscus flower. The density of the sponges is determined as 0.027–0.068 g/cm^3 (Fig. 3B). The low density is due primarily to the fact that the water in the sample is replaced by air during the freeze-drying process and a sponge-like porous material is formed. The density of the composite sponges increases linearly with the increase of CB. When the amount of CB is 200%, the density of the composite sponge material is about three times of pure CS sponge. However, the addition of CB does not have much impact on the porosity of sponges and all sponges maintain 82.1 ± 9.0% porosity. The slight effect on the porosity of CS sponges by addition of CB is due to the slightly changed water content in the same volume solution. The similar trend in porosity of CS

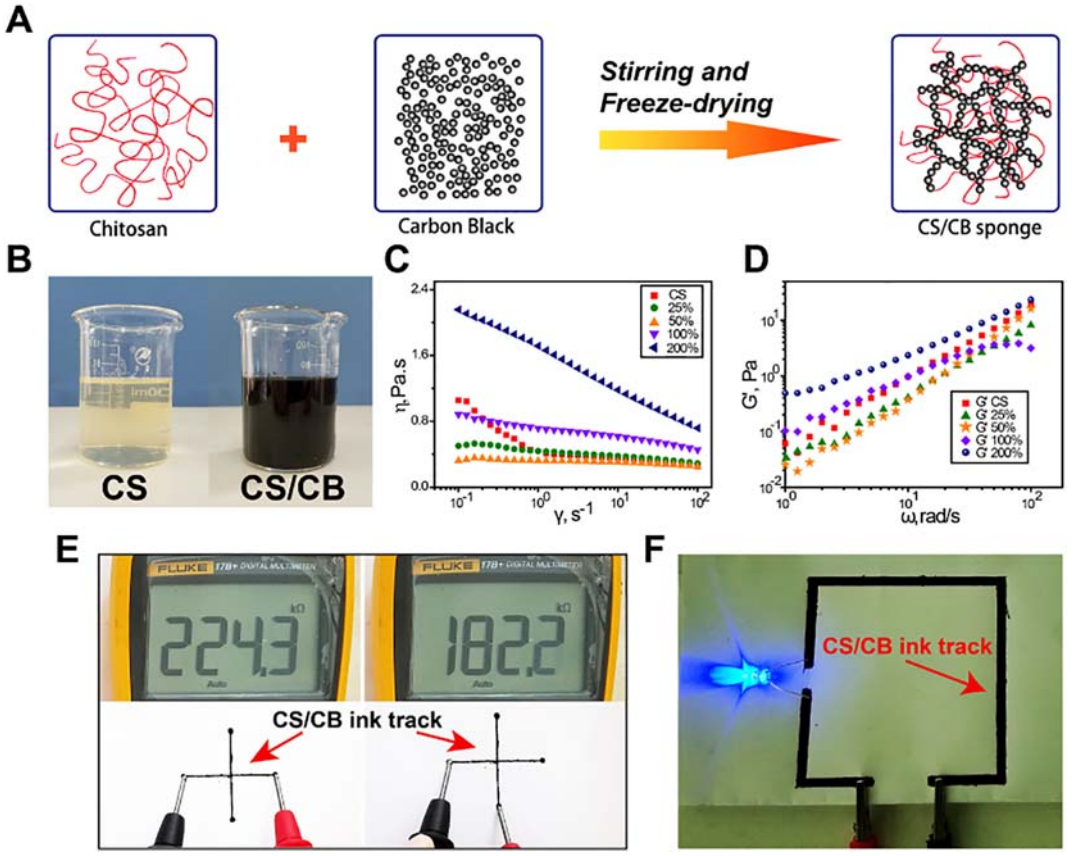

Fig. 2. The preparation process of CS/CB composite sponge (A); The appearance of pure CS and CS/CB solution (B); The dynamic viscosity of different concentrations of CS/CB solutions (C); The shear modulus (G', elastic component) of different concentrations of CS/CB solution (D); Writing traces and resistance measurements of CS/CB solution on A4 paper (E); A simple circuit diagram on A4 paper draw by ballpoint pens loaded with CS/CB solution (F).

composite sponges has also been found in other composite systems [33, 34].

Fig. 3C compares the conductivity of CS/CB composite sponges. Pure CS sponge is insulated and CS/CB composite sponge is electrically conductive. When the composite sponge connects to the circuit, the bulb in the circuit can emit light (inset in Fig. 3C). It can be seen that the addition of CB enhances the conductivity of the composite sponge significantly. For example, when the content of CB is 25%, the conductivity of the composite sponge is only 215 μS/cm. When the CB content is 100%, the conductivity of the composite sponge reaches 8308 μS/cm. The significant increase in the conductivity of the CS sponge indicates that CB network is built in the composites. When the CB content is 200%, the conductivity of the composite sponges further increases. However, the viscosity of the CB/CS mixture solution at high CB loading is too high, so it is not easy to pour into the molds during the preparation process of the sponges. Therefore, the 200% CB content was selected as the maximum content in the present study. The conductivity determination results suggest that the addition of CB into CS can make the composite sponges be conductive.

Fig. 3D shows the appearances and compressive strain-stress curves of the pure CS and CS/CB composite sponges. The compressive modulus and compressive strength of the composite sponge increase with the increase of the amount of CB. The addition of a small amount of CB does not result in the significant increase in compressive modulus of composite sponges. When the addition amount is 25%, the composite sponge has a compressive strength of 62.3 kPa. When the amount of CB increases, the compressive strength rises sharply. For example, the stress at deformation of 20%, 40%, 60% of composite sponge with 200% CB shows 4.27, 4.04, and 4.55 folds compared with pure CS sponge. The reinforcement effect of CB towards CS is attributed to the nanoscale size of CB and the interactions between CS chains and surface groups of CB.

In order to determine the effect of CB on the microstructure of CS sponges, XRD and IR experiments were conducted. Fig. 3E shows the XRD patterns of CS sponge and CS/CB composite sponges. It can be seen that CS exhibit a strong peak at $2\theta = 23°$ and a weak peak at $2\theta = 10°$, which is in agreement with the previously reported [35]. CB exhibits two characteristic peaks around 26 and 43° [27]. It can be found that the characteristic peak of CS at 23° and the characteristic peak of CB around 26° are overlapped in the composite sponges. More CB in the composite sponges is, more similar of the peak with CB alone is. Fig. 3F shows the IR spectra of CS, CB, and CS/CB composite sponges. In the spectrum of pure CS, the peak around 3438 cm^{-1} is assigned to the intermolecular –OH stretching vibration. The absorption peak at 1650 cm^{-1} is the characteristic peak of the amide I band, and the shoulder peak at 1602 cm^{-1} is -NH_2 bending vibration (amide II band). In the spectra of CS/CB composite sponges, the peak transfers from CS to CB gradually with the increase in CB content. This should be attributed to the fact that CB particles can cover the CS chains and CB has a strong absorption towards the infrared light. Moreover, the –OH stretching vibration peak located in 3000–37,00 cm^{-1} nearly disappear in the composite sponges, suggesting interfacial interactions between CS and CB. It also should be noted that the IR test was performed using infrared attenuated total reflection mode. So, the absorption peak of CS is covered by the characteristic peaks of CB.

Fig. 3G shows the TGA curves of CS and CS/CB composite sponges. The thermal decomposition of CS can be divided into two processes. The weight loss before 250 °C is caused by the thermal evaporation of the bound water, crystalline water, and residual acetic acid in the sponges. After that, the thermal decomposition of the CS chains occurs at 250–540 °C and the thermal degradation ends at ~550 °C. All curves of CS/CB composites are above that of CS (expect the CS/CB composite with 25% CB before 250 °C) suggest that the addition of CB can improve

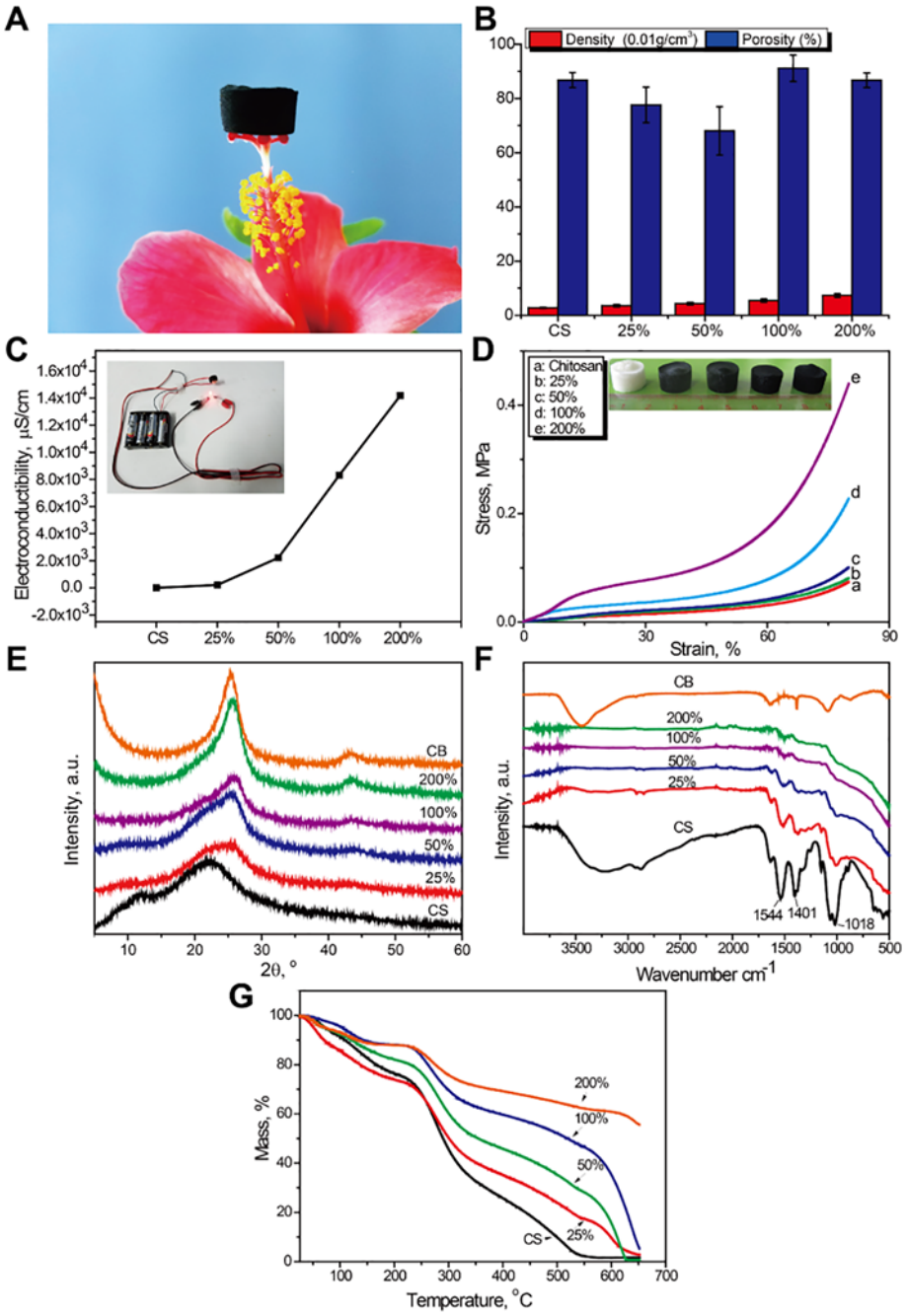

Fig. 3. The appearance of CS/CB composite sponge standing on pistils of Hibiscus flower (A); The density and porosity of CS/CB composite sponges (B); The conductivity of CS/CB composite sponges (the inset shows the bulb linked with CS/CB composite sponge in the circuit can emit light) (C); The compressive stress-strain curve of CS/CB composite sponges (the inset shows the appearance of CS and CS/CB composite sponges) (D); XRD patterns of CS/CB composite sponges (E); FTIR spectra of CS/CB composite sponges (F); TG curves of CS/CB composite sponges (G).

the thermal stability of CS. CB does not alter the decomposition temperature of CS but reduces the thermal decomposition rate of CS. Another difference is that an obvious weight loss is found in the CS/CB composite sponge after 600 °C. This is primarily due to the fact that the CB can release hydrogen, carbon monoxide, carbon dioxide, and other gas volatile when it is heated to 400–1000 °C under anoxic conditions. Volatile comes from the decomposition of C—H bonds on the CB surfaces.

3.4. The microstructure of CS/CB composite sponges

In order to examine the pore structure and the dispersion state of CB in the CS matrix, an examination of the fractured surface of CS/CB composite sponges was carried out using SEM. As is shown in Fig. 4, pure CS sponge and CS/CB composite sponge exhibit three-dimensional pore structure with pore size between 50 and 100 μm. The surfaces of the pore wall in pure CS sponge are very smooth, while the surfaces of the pore wall in CS/CB composite sponges are rough. In the 200 X photographs, it is obviously seen that CB particles appear in the surfaces of CS/CB composite sponges. This indicates that CB particles have been successfully decorated on the surfaces of CS sponge and they constitute an interconnected conductive network. The greater the amount of CB is, the more rough of the surfaces. CB particles can form continuous conductive network, so the conductivity is enhanced. In addition, the introduction of CB makes pore walls of the sponges be thicker. The thick pore walls can tolerate loading, therefore the compression performance of CS/CB composite sponges is significantly improved. However, if the CB

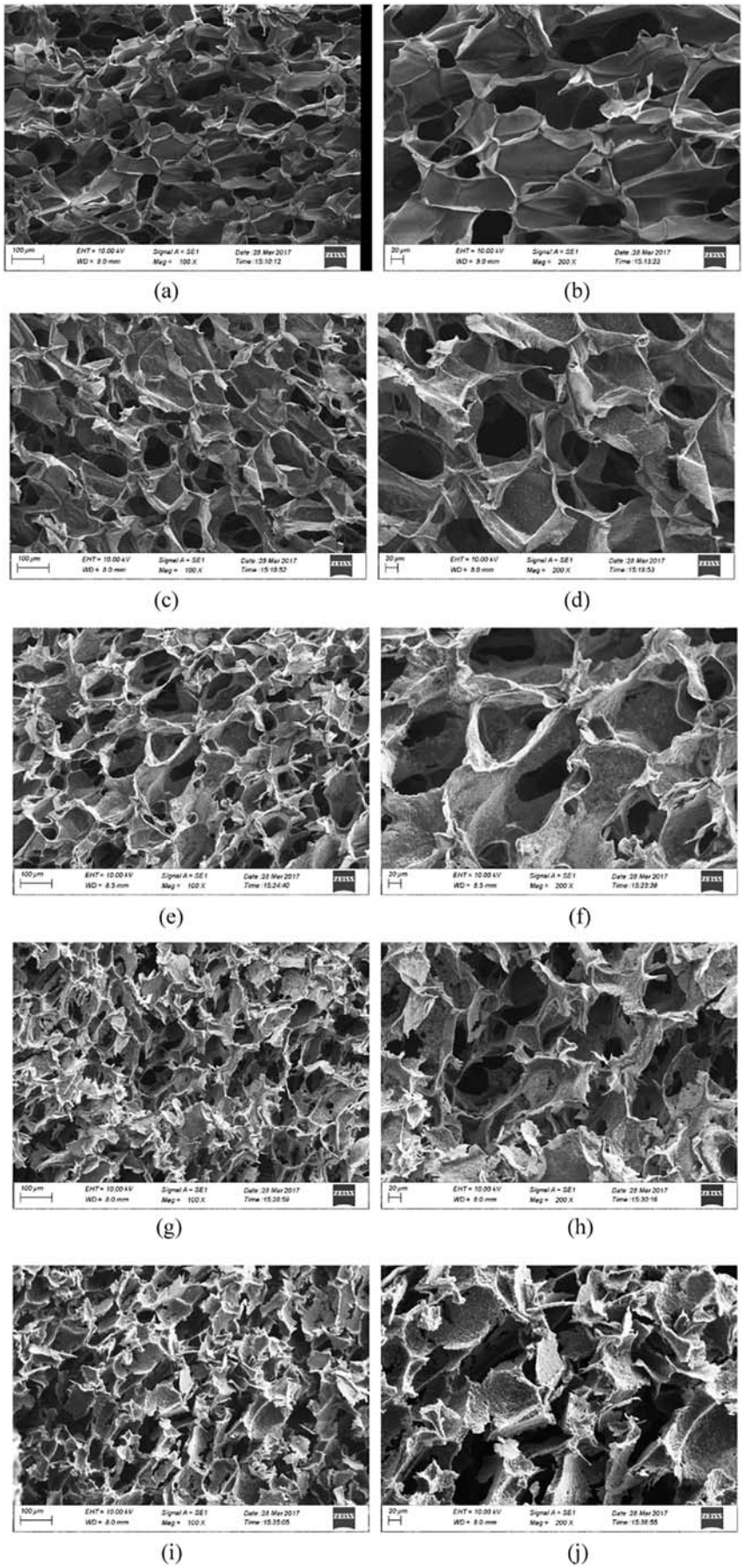

Fig. 4. SEM images of fractured surface for CS/CB composite sponges: (a) and (b) pure CS; (c) and (d) 25%; (e) and (f) 50%; (g) and (h) 100%; (i) and (j) 200%.

content further increases, the sponges become brittle due to the weakened interfacial bonding. For example, when the content of CB is 300%, the structure of the sponges is unstable and CB is easy to drop from the CS/CB composite sponges. However, in CB content range of 25%–200%, the adhere strength of the CB on the walls of CS of the composites sponges is satisfied for the application as strain sensor. No CB falls off from the sponges due to the interfacial interactions between CS and CB shown in previous FITR result.

3.5. Performance of the CS/CB composite sponge strain sensor

The conductive CS/CB composite sponges can be used as strain sensors to detect human physiological activities in real time, especially small-scale movements such as pronunciation, breathing, and so on. The ability of CS/CB composite sensor in detecting delicate motions of the throat during pronouncing was firstly evaluated. The striped CS/CB sponge sample is fixed to the neck to detect the muscle motions of the vocal cords of a tester. During the pronunciation, resistance changes were recorded by an electrical analyzer (Fig. 5A). When the tester pronounces different words, the CS/CB strain sensor exhibits distinct current patterns relating to their pronunciation since each word causes particular movement of the vocal muscle. For example, pronunciation of the single syllable word “Hi” displays a single peak signal, while a big peak with a linked small peak are found in the two-syllable word “Hello”. There are three signal peaks in the three syllable word “wonderful” pronunciation. The intensity of the current is related to the strength of syllables. The pronunciation of different words will make the vocal cord muscles occur different movements, and the conductive CS/CB composite sponges can record varying degrees of the deformation. The sensitivity of a strain sensor usually is shown in terms of its gauge factor (GF) defined as $GF = (\Delta R/R_0)/\varepsilon$, where ΔR is the resistance change with straining, R_0 the resistance before straining, and ε the applied strain. From the detecting throat vibration which is a very tiny deformation (~1.33%), the composite sponges can cause a ~10% resistance change immediately. Therefore, the average GF of the sponges is estimated to be ~7.5 which is comparable to previously reported conductive CB composite systems [36]. Also, when one word is repeatedly pronounced, nearly invariable current patterns are recorded, suggesting the reliability of the sensor. Therefore, CS/CB composite sponges can judge the number of syllables in some simple words through the monitoring of the electrical signals, which indicates that CS/CB composite sponges have great potentials in sound monitoring and recognition.

The CS/CB composite sponge was further developed as a sensor for detecting breathing. To prepare a simple breathing monitoring device, the CS/CB composite strip sponges was fixed to the belt buckle through the adhesive tape (Fig. 5B). The sensor device was then bound to the waist of the tester, and the resistance was recorded in real time. During the respiratory test, when the volunteer inhale, the abdominal bulging causes the sponge to be compressed. At this time, CB conductive network in the composite sponge comes in contact with each other due to extrusion, so the electric conductivity is enhanced. As a result, the resistance decreases and a signal peak is recorded in Fig. 5C. In contrast, when the tester exhales, the abdomen relaxation and the deformation of sponges recover. Meanwhile, CB network is restored, so the resistance increases and goes back to the initial state. In the multiple cycle experiments, the relative resistance change rate shows a good linear response and stability. The experimental results suggest that CS/CB composite sponge has good reversibility and repeatability in tiny compressive strain sensing.

In order to investigate the response of CS/CB composite sponge to bending strain, the strip CS/CB composite sponge samples were fixed on the finger and arm joints respectively. The volunteer was subjected to repeated bending-stretching action and the real-time resistance of the samples was recorded. Fig. 6A shows that the volunteers wear rubber gloves and the strip CS/CB composite sponge was fixed on the articular surface of the index finger. The volunteer repeatedly did bending-unbending action of the index finger. When the index finger bends, the resistance of the composite sponges appears to significantly reduce

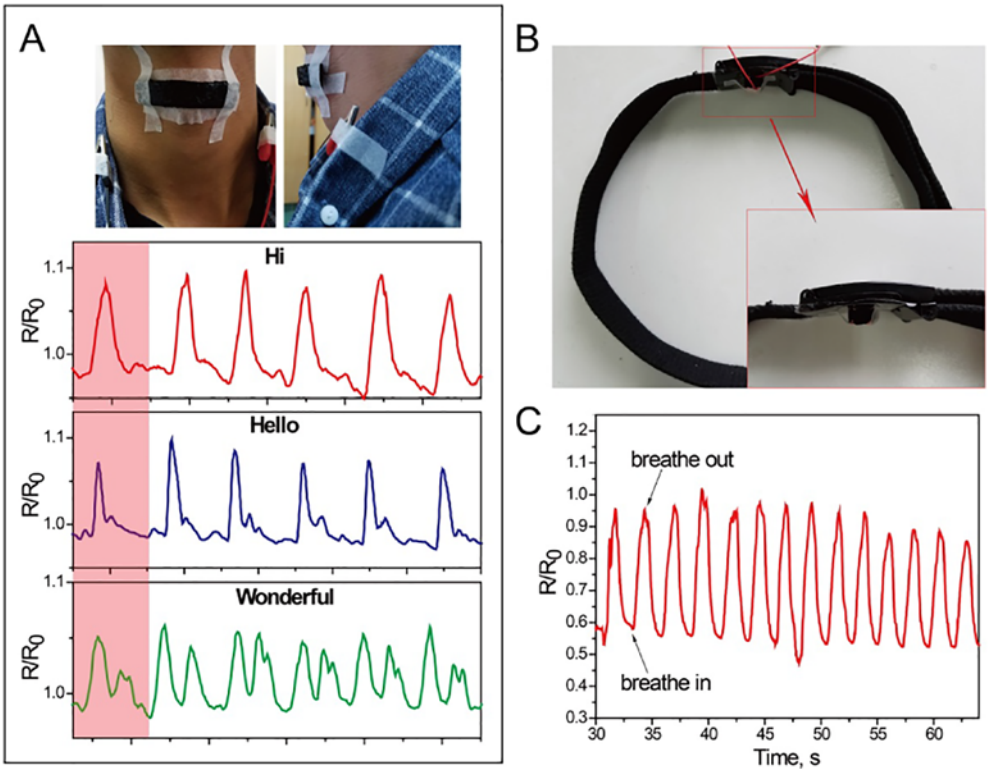

Fig. 5. Photograph of the CS/CB strain sensor directly attached on the neck and the recorded resistant variations of the CS/CB sensor with the tester pronouncing different words: Hi, Hello, and Wonderful, respectively (A); Photograph of the CS/CB strain sensor for detecting breathing (B); The recorded resistant variations of the CS/CB sensor with the tester breathing (C).

due to the stretching of the conductive network. During unbending fingers, the resistance recovers to its original level, resulting from the reestablishment of the conductive network in the composite. It can be observed that the signal produced by the bending and unbending of the index finger is kept at a high degree of similarity, which indicates that the CS/CB composite sponge has superior sensitivity and stable electrical response to the physical movement of the human body. Similarly, the strip CS/CB composite sponge was fixed to the volunteer's arm joint, and then the volunteer repeated the bending-stretching movement of the arm. Also, the real-time resistance of the sample was recorded with a resistance tester. The response of resistance signal peaks is illustrated in Fig. 6B. The principle of the signal peak appears similar to the bending and extension movement of the finger, and the squeeze of the joint sponge material leads to a decrease in resistance.

The sensor stability of CS/CB composite sponges shows practical significance as a strain sensor. Cyclic stability is a better indication of the reliability of the electrical parameters of the sensor. The strip CS/CB sample was fixed at the angle of the cover of the notebook, and the notebook was repeatedly opened and closed (Fig. 6C). The resistance was recorded in real time by the resistance tester. The results of the test are presented in Fig. 6D. The resistance of the CS/CB composite sponge exhibits good repeatability after 200 bending-recovery cycles without obvious changed resistance. The resistance at the termination point is basically the same, indicating that CS/CB composite sponge in the cycle still has good stability. However, the resistance change ratio of the composite sponge in the later period of the cycle shifts to a higher degree, which is due to that the stress applied to the composite sponge in the process of bending causes the stress relaxation of the polymer chains. Another possible reason for this is the circulation causes the CB conductive network destroys or deforms partly. Since the damage or deformation of conductive CB network is unable to be repaired by itself, baseline offset is found in the R/R_0 curves. Also, the cycle process operated by hand also may bring some offset. In total, all results demonstrate that CS/CB composite sponge has good sensitivity, reversibility, and repeatability in strain sensing, which shows great potential as low cost sensors in detecting human motions.

4. Conclusions

CS/CB composite porous sponge is prepared by combining solution-mixing and freeze-drying techniques. CS/CB solution is a non-Newtonian pseudoplastic fluid which shows shear thinning behavior. The viscosity, shear modulus, and the conductivity of CS/CB composite increase with the loading of CB. The CS/CB conductive ink can be written on A4 paper by a pen, which shows high electric conductivity. The addition of CB improves the compressive strength and thermal stability of CS. The conductivity of CS/CB composite sponge with 200% CB content reaches to 1.4×10^4 μS/cm. XRD and IR results show the two components are successfully compounded without structural change. The addition of CB leads to a slight decrease in the porosity of CS sponges. CS/CB composite sponges can be utilized to detect various human activities (such as pronouncing, breathing, and joint bending), and they show good sensitivity and stability after several hundred loops. The advantages of low-cost, easy fabricating process, flexible, and high performance of CS/CB composite sponges make them have great potentials in highly sensitive strain sensor.

Acknowledgments

This work was financially supported by National High Technology Research and Development Program of China (2015AA020915), National Natural Science Foundation of China (51473069 and 51502113), and

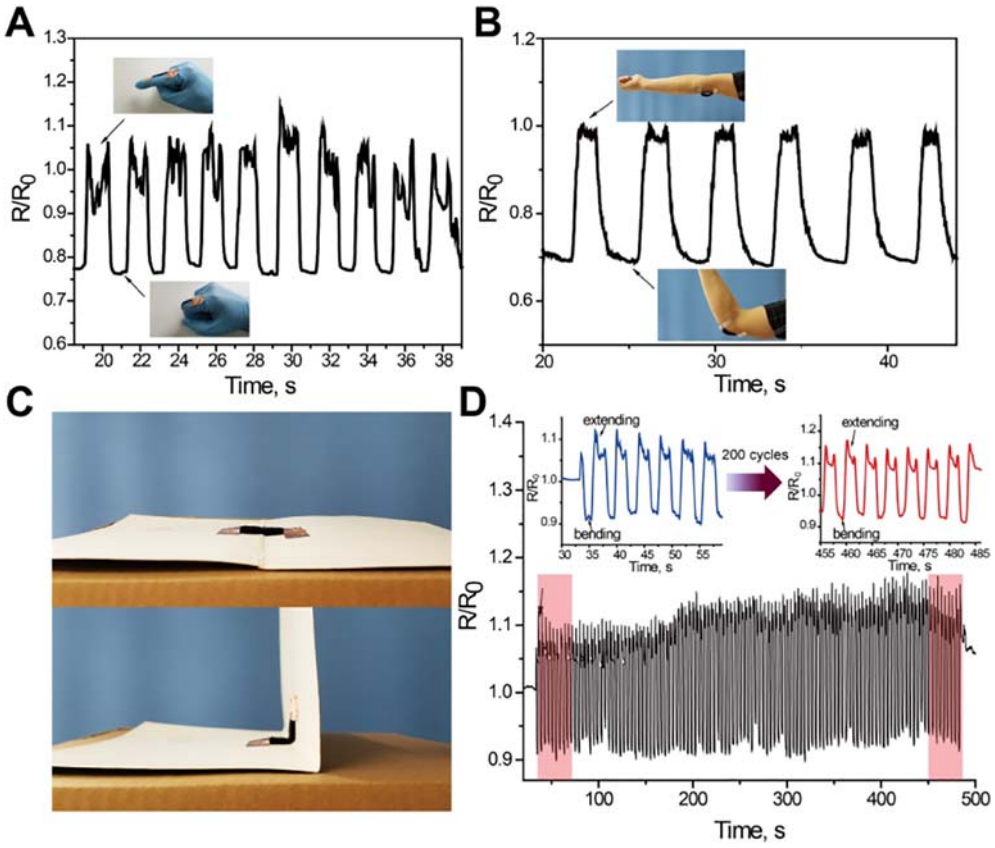

Fig. 6. Representative resistant signal of the CS/CB sensors during bending and unbending index finger (A); Representative resistant signal of the CS/CB sensors during flexion and extension of arm (B); Photograph of the CS/CB strain sensor attached to the angle of the cover of the notebook (C); Cycle stability test of CS/CB composite sponge during bending and extending of the notebook (D).

the Guangdong Natural Science Funds for Distinguished Young Scholar (S2013050014606), Guangdong Special support program (2014TQ01C127), Science and Technology Planning Project of Guangdong Province (2014A020217006), the Pearl River S&T Nova Program of Guangzhou (201610010026).

Appendix A. Supplementary data

Supplementary data to this article can be found online at https://doi.org/10.1016/j.matdes.2017.12.046.

References

[1] J. Wang, H. Sato, C.Y. Xu, M. Taya, Bioinspired design of tactile sensors based on Flemion, J. Appl. Phys. 105 (2009), 083515.
[2] X.D. Wu, Y.Y. Han, X.X. Zhang, Z.H. Zhou, C.H. Lu, Large-area compliant, low-cost, and versatile pressure-sensing platform based on microcrack-designed carbon black@ polyurethane sponge for human–machine interfacing, Adv. Funct. Mater. 26 (2016) 6246–6256.
[3] H. Cao, S.K. Thakar, M.L. Oseng, C.M. Nguyen, C. Jebali, A.B. Kouki, J.C. Chiao, Development and characterization of a novel interdigitated capacitive strain sensor for structural health monitoring, IEEE Sensors J. 15 (2015) 6542–6548.
[4] Y.C. Lai, B.W. Ye, C.F. Lu, C.T. Chen, M.H. Jao, W.F. Su, W.Y. Hung, T.Y. Lin, Y.F. Chen, Extraordinarily sensitive and low-voltage operational cloth-based electronic skin for wearable sensing and multifunctional integration uses: a tactile-induced insulating-to-conducting transition, Adv. Funct. Mater. 26 (2016) 1286–1295.
[5] H. Yousef, M. Boukallel, K. Althoefer, Tactile sensing for dexterous in-hand manipulation in robotics—a review, Sensors Actuators A 167 (2011) 171–187.
[6] C.L. Choong, M.B. Shim, B.S. Lee, S. Jeon, D.S. Ko, T.H. Kang, J. Bae, S.H. Lee, K.E. Byun, J. Im, Highly stretchable resistive pressure sensors using a conductive elastomeric composite on a micropyramid array, Adv. Mater. 26 (2014) 3451–3458.
[7] S. Ryu, P. Lee, J.B. Chou, R. Xu, R. Zhao, A.J. Hart, S.G. Kim, Extremely elastic wearable carbon nanotube fiber strain sensor for monitoring of human motion, ACS Nano 9 (2015) 5929–5936.
[8] Q. Sun, D.H. Kim, S.S. Park, N.Y. Lee, Y. Zhang, J.H. Lee, K. Cho, J.H. Cho, Transparent, low-power pressure sensor matrix based on coplanar-gate graphene transistors, Adv. Mater. 26 (2014) 4735–4740.
[9] S. Lim, D. Son, J. Kim, Y.B. Lee, J.K. Song, S. Choi, D.J. Lee, J.H. Kim, M. Lee, T. Hyeon, Transparent and stretchable interactive human machine interface based on patterned graphene heterostructures, Adv. Funct. Mater. 25 (2015) 375–383.
[10] Y.A. Samad, Y.Q. Li, S.M. Alhassan, K. Liao, Novel graphene foam composite with adjustable sensitivity for sensor applications, ACS Appl. Mater. Interfaces 7 (2015) 9195–9202.
[11] S. Gong, W. Schwalb, Y.W. Wang, Y. Chen, Y. Tang, J. Si, B. Shirinzadeh, W.L. Cheng, A wearable and highly sensitive pressure sensor with ultrathin gold nanowires, Nat. Commun. 5 (2014) 3132.
[12] G.O. Shonaike, S.G. Advani, Advanced Polymeric Materials: Structure Property Relationships, CRC Press, 2003.
[13] H. Liu, J.C. Gao, W.J. Huang, K. Dai, G.Q. Zheng, C.T. Liu, C.Y. Shen, X.R. Yan, J. Guo, Z.H. Guo, Electrically conductive strain sensing polyurethane nanocomposites with synergistic carbon nanotubes and graphene bifillers, Nano 8 (2016) 12977–12989.
[14] X. Yuan, Y. Wei, S. Chen, P.P. Wang, L. Liu, Bio-based graphene/sodium alginate aerogels for strain sensors, RSC Adv. 6 (2016) 64056–64064.
[15] X.D. Wu, Y.Y. Han, X.X. Zhang, C.H. Lu, Highly sensitive, stretchable, and wash-durable strain sensor based on ultrathin conductive layer@ polyurethane yarn for tiny motion monitoring, ACS Appl. Mater. Interfaces 8 (2016) 9936–9945.
[16] Y. Lin, S.Q. Liu, S. Chen, Y. Wei, X.H. Dong, L. Liu, A highly stretchable and sensitive strain sensor based on graphene–elastomer composites with a novel double-interconnected network, J. Mater. Chem. C 4 (2016) 6345–6352.
[17] N. Hauptman, A. Vesel, V. Ivanovski, M.K. Gunde, Electrical conductivity of carbon black pigments, Dyes Pigments 95 (2012) 1–7.
[18] S. Matchawet, A. Kaesaman, P. Bomlai, C. Nakason, Electrical, dielectric, and dynamic mechanical properties of conductive carbon black/epoxidized natural rubber composites, J. Compos. Mater. 50 (2016) 2191–2202.
[19] X.H. Guo, Y. Huang, X. Cai, C.X. Liu, P. Liu, Capacitive wearable tactile sensor based on smart textile substrate with carbon black/silicone rubber composite dielectric, Meas. Sci. Technol. 27 (2016), 045105.
[20] M. Baccarin, F.A. Santos, F.C. Vicentini, V. Zucolotto, B.C. Janegitz, O. Fatibello-Filho, Electrochemical sensor based on reduced graphene oxide/carbon black/chitosan composite for the simultaneous determination of dopamine and paracetamol concentrations in urine samples, J. Electroanal. Chem. 799 (2017) 436–443.
[21] M.L. Huang, L.B. Tunnicliffe, J. Zhuang, W. Ren, H.X. Yan, J.J. Busfield, Strain-dependent dielectric behavior of carbon black reinforced natural rubber, Macromolecules 49 (2016) 2339–2347.
[22] K. Princy, R. Joseph, C.S. Kartha, Studies on conductive silicone rubber compounds, J. Appl. Polym. Sci. 69 (1998) 1043–1050.
[23] W. Luheng, D. Tianhuai, W. Peng, Influence of carbon black concentration on piezoresistivity for carbon-black-filled silicone rubber composite, Carbon 47 (2009) 3151–3157.
[24] X.D. Wu, C.H. Lu, Y.Y. Han, Z.H. Zhou, G.P. Yuan, X.X. Zhang, Cellulose nanowhisker modulated 3D hierarchical conductive structure of carbon black/natural rubber nanocomposites for liquid and strain sensing application, Compos. Sci. Technol. 124 (2016) 44–51.
[25] E.S. Bhagavatheswaran, M. Parsekar, A. Das, H.H. Le, S. Wiessner, K.W. Stöckelhuber, G. Schmaucks, G. Heinrich, Construction of an interconnected nanostructured carbon black network: development of highly stretchable and robust elastomeric conductors, J. Phys. Chem. C 119 (2015) 21723–21731.
[26] T. Ungár, J. Gubicza, G. Ribárik, C. Pantea, T.W. Zerda, Microstructure of carbon blacks determined by X-ray diffraction profile analysis, Carbon 40 (2002) 929–937.
[27] P.A. Thrower, Chemistry & Physics of Carbon, CRC Press, 1996.
[28] W.W. Simons, Sadtler Handbook of Infrared Spectra, Sadtler research laboratories, 1978.
[29] C. Portet, G. Yushin, Y. Gogotsi, Electrochemical performance of carbon onions, nanodiamonds, carbon black and multiwalled nanotubes in electrical double layer capacitors, Carbon 45 (2007) 2511–2518.
[30] A. Sadezky, H. Muckenhuber, H. Grothe, R. Niessner, U. Pöschl, Raman microspectroscopy of soot and related carbonaceous materials: spectral analysis and structural information, Carbon 43 (2005) 1731–1742.
[31] E. Ustinov, D. Do, V. Fenelonov, Pore size distribution analysis of activated carbons: application of density functional theory using nongraphitized carbon black as a reference system, Carbon 44 (2006) 653–663.
[32] Y. Wei, S.L. Chen, F.C. Li, Y. Lin, Y. Zhang, L. Liu, Highly stable and sensitive paper-based bending sensor using silver nanowires/layered double hydroxides hybrids, ACS Appl. Mater. Interfaces 7 (2015) 14182–14191.
[33] M.X. Liu, C.C. Wu, Y.P. Jiao, S. Xiong, C.R. Zhou, Chitosan–halloysite nanotubes nanocomposite scaffolds for tissue engineering, J. Mater. Chem. B 1 (2013) 2078–2089.
[34] M.X. Liu, H.J. Zheng, J. Chen, S.L. Li, J.F. Huang, C.R. Zhou, Chitosan-chitin nanocrystal composite scaffolds for tissue engineering, Carbohydr. Polym. 152 (2016) 832–840.
[35] Y.H. Yang, J.H. Cui, M.T. Zheng, C.F. Hu, S.Z. Tan, Y. Xiao, Q. Yang, Y.L. Liu, One-step synthesis of amino-functionalized fluorescent carbon nanoparticles by hydrothermal carbonization of chitosan, Chem. Commun. 48 (2012) 380–382.
[36] J.H. Kong, N.S. Jang, S.H. Kim, J.M. Kim, Simple and rapid micropatterning of conductive carbon composites and its application to elastic strain sensors, Carbon 77 (2014) 199–207.